Stability Enhancement of DFIG-Based Offshore Wind Farm Fed to a Multi-Machine System Using a STATCOM

Li Wang, *Senior Member, IEEE*, and Dinh-Nhon Truong

***Abstract*—In this paper, the simulation results of using a static synchronous compensator (STATCOM) to achieve damping improvement of an offshore wind farm (OWF) fed to a multi-machine system is presented. The operating performance of the studied OWF is simulated by an equivalent aggregated doubly-fed induction generator (DFIG) driven by an equivalent aggregated wind turbine (WT) through an equivalent gearbox. A PID damping controller and a hybrid PID plus fuzzy logic controller (FLC) of the proposed STATCOM are designed to contribute adequate damping characteristics to the dominant modes of the studied system under various operating conditions. A frequency-domain approach based on a linearized system model using root-loci technique and a time-domain scheme based on a nonlinear system model subject to a three-phase short-circuit fault at the connected bus are systematically performed to examine the effectiveness of the proposed control schemes. It can be concluded from the comparative simulated results that the proposed STATCOM joined with the designed hybrid PID plus FLC is shown to be superior for improving the stability of the studied system subject to a severe disturbance than the PID controller.**

***Index Terms*—Doubly-fed induction generator, fuzzy logic controller, multi-machine system, offshore wind farm, stability, static synchronous compensator.**

I. Introduction

DOUBLY-FED induction generator (DFIG) is, currently, the most employed wind generator due to its several merits. One of the advantages is the higher efficiency compared to a direct-drive wind power generation system with full-scale power converters since only about 20% of power flowing through power converter and the rest through stator without power electronics. Another advantage of a wind DFIG is the capability of decoupling control of active power and reactive power for better grid integration [1]. However, by connecting stator windings directly to the power grid, a wind DFIG is extremely sensitive to grid faults. Moreover, wind energy is a kind of stochastic energy, implying that the output of OWF varies in a certain range due to unstable wind characteristic. Therefore, the operating point of the power system changes from time to time when the wind power is integrated with the power system. Several published papers have discussed how to reduce the negative influences of the power grid on DFIG-based wind farms [2]–[6]. In [2], DFIG-based OWF connected to a power grid through a line-commutated high-voltage direct-current (HVDC) with a damping controller located at the rectifier current regulator of the HVDC link was proposed to contribute adequate damping to the OWF under various wind speeds and different disturbance conditions. But this control scheme was only suitable for the systems having a long distance from OWFs to onshore grids. In [3], a variable frequency transformer (VFT) was proposed to smooth the fluctuating active power generated by the OWF sent to the power grid and improve the damping of the OWF. These papers, however, just considered a power grid as an infinite bus that is not a practical power system.

To study the performance of a practical power system, a multi-machine power system is generally employed to replace the single-machine infinite-bus (SMIB) equivalent model. In [4], a DFIG-based wind power plant (WPP) was connected to a three-machine nine-bus system to compare voltage stability of the system at a point of common coupling when the system was with and without the WPP. The dynamic performance of DFIG-based wind turbines connected to multi-machine systems under three different configurations was presented in [5]. A new control strategy for improving fault ride-through capability of wind farms connected to a multi-machine power system was proposed in [6], while a small series dynamic braking resistor was located at the stator circuit of the DFIG along with a DC-chopper braking resistor. Especially, increase of wind-power penetration could lead to the problem of sudden disconnection of considerable amount of power generation in case of a transient fault occurred in the system, causing the system to be unstable from an otherwise harmless fault situation. In this case, a static synchronous compensator (STATCOM) is one of the good candidates for dynamic compensation of reactive power when the voltage is lower than the normal voltage range. A STATCOM can generate more reactive power than other FACTS devices like static VAR compensator (SVC). This is due to the fact that the maximum capacitive power generated by a STATCOM decreases only linearly with the bus voltage but it drops off as square of the bus voltage for an SVC. In addition, the STATCOM normally exhibits a faster response as it has no significant time delay associated with thyristor firing (in the order of 4 ms for an SVC) [7]. In [8], a STATCOM was connected at the point of common coupling (PCC) to maintain stable voltage and to improve the power quality by protecting DFIG-based wind farm connected to a weak grid from going offline during and

Manuscript received June 12, 2012; revised September 30, 2012, November 14, 2012, and January 13, 2013; accepted February 15, 2013. Date of publication March 15, 2013; date of current version July 18, 2013. This work was supported by the National Science of Council (NSC) of Taiwan under Grant NSC 101-3113-P-006-014. Paper no. TPWRS-00652-2012.

L. Wang is with the Department of Electrical Engineering as well as the Research Center for Energy Technology and Strategy, National Cheng Kung University, Tainan City 70101, Taiwan (e-mail: liwang@mail.ncku.edu.tw).

D.-N. Truong is with the Department of Electrical Engineering, National Cheng Kung University, Tainan City 70101, Taiwan (e-mail: nhontd@yahoo.com).

Color versions of one or more of the figures in this paper are available online at http://ieeexplore.ieee.org.

Digital Object Identifier 10.1109/TPWRS.2013.2248173

0885-8950/$31.00 © 2013 IEEE

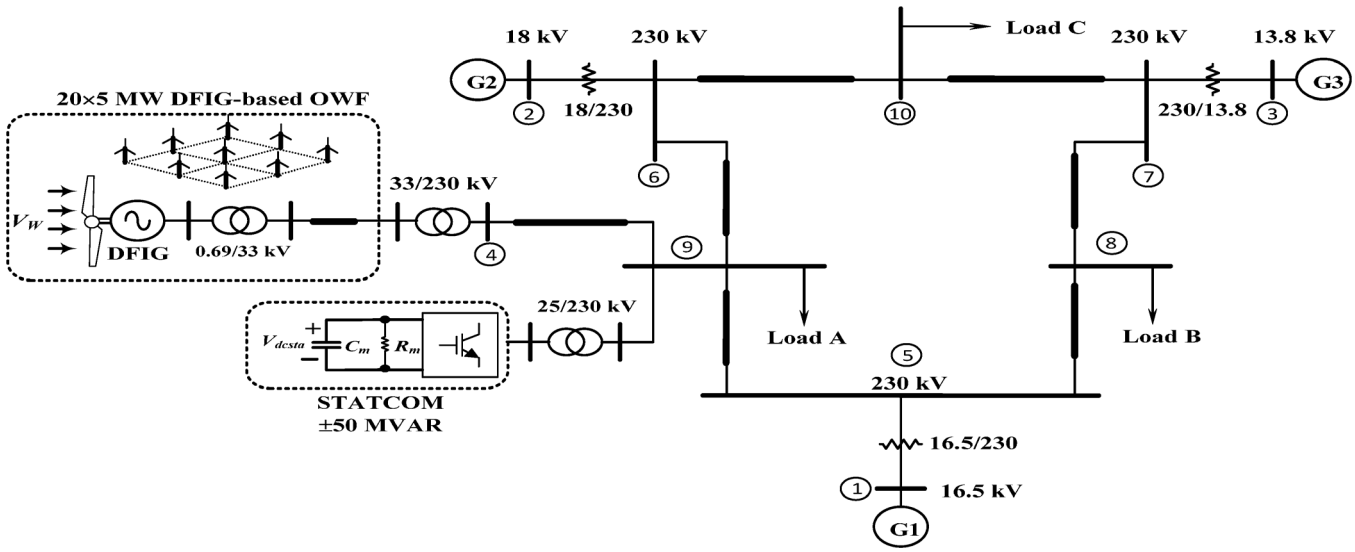

Fig. 1. Configuration of the studied system.

after disturbances. As proposed in [9], a new control strategy using a full-power wind permanent-magnet generator (PMG) with a STATCOM to provide reactive power compensation can be used to improve stability of transient voltage. In [10], performance of a PMG-based wind energy system employing a dynamic voltage regulator (DVR) was compared to one of the system employing a STATCOM. It is recommended to use a STATCOM in systems with large loads where reactive power consumption from the grid could cause serious effects on connected loads. Also in [11], a STATCOM with a fuzzy logic controller (FLC) was used to enhance power stability of a two-area four-generator interconnected power system. Co-operating a PI controller and an FLC applied to improve dynamic and steady-state performance of a speed controller based interior permanent-magnet synchronous motor was proposed in [12]. Simulation and experimental results were demonstrated that the superior performance of the proposed hybrid control over conventional fixed-gain PI controller. The tuning of the scaling factors of a fuzzy PID-type controller with other fuzzy systems used in the excitation control of a synchronous power generator connected to an infinite bus through a transmission line was proposed in [13]. It was found that PID and fuzzy controller combinations can produce a better quality control. For the purpose of improving the damping of the studied power system for grid integration of an OWF, this paper proposes a STATCOM connected to the interconnected bus of a DFIG-based OWF fed to a three-machine nine-bus system for compensating reactive power and maintaining the voltage at the connected bus. The main contribution of this study is the hybrid PID plus FLC considered as a new damping controller which is designed to damp out oscillations of the studied system.

This paper is organized as below. System configuration and employed models for the studied DFIG-based OWF fed to a three-machine nine-bus system using a STATCOM are introduced in Section II. The design procedure and design results for the PID damping controller of the proposed STATCOM using pole-placement technique and the designed FLC plus the PID are depicted in Section III. Root-loci results of system dominant modes under various operation points as well as comparative transient responses of the studied system with and without the designed PID and the hybrid PID plus FLC damping controllers subject to severe disturbance are described in Sections IV and V, respectively. Finally, specific important conclusions of this paper are drawn in Section VI.

II. System Configuration and Mathematical Models

Fig. 1 shows the configuration of the studied system. A DFIG-based OWF of 100 MW and a STATCOM of ±50-MVAR are connected to bus 9 of a three-machine nine-bus system. The OWF is represented by a large equivalent aggregated DFIG driven by an equivalent aggregated variable-speed wind turbine (VSWT) through an equivalent gearbox. The employed mathematical models of the studied system are described as below.

A. Wind Turbine

The captured mechanical power (in W) by a VSWT can be written by

$$P_m = \frac{1}{2}\rho \cdot A_r \cdot V_W^3 \cdot C_p(\lambda, \beta) \tag{1}$$

where ρ is the air density $(\mathrm{kg/m^3})$, A_r is the blade impact area $(\mathrm{m^2})$, V_W is the wind speed (m/s), and C_p is the dimensionless power coefficient of the VSWT. The power coefficient of the VSWT C_p is given by

$$C_p(\psi_k, \beta) = c_1\left(\frac{c_2}{\psi_k} - c_3 \cdot \beta - c_4 \cdot \beta^{c_5} - c_6\right)\exp\left(-\frac{c_7}{\psi_k}\right) \tag{2}$$

in which

$$\frac{1}{\psi_k} = \frac{1}{\lambda + c_8\beta} - \frac{c_9}{\beta^3 + 1} \tag{3}$$

$$\lambda = \frac{R_{bld}\omega_{bld}}{V_W} \tag{4}$$

where ω_{bld} is the blade angular speed (rad/s), R_{bld} is the blade radius (m), λ is the tip speed ratio, β is blade pitch angle (degrees), and $c_1 - c_9$ are the constant coefficients for power coefficient C_p. The wind speed V_W is modeled as the algebraic sum of a base wind speed, a gust wind speed, a ramp wind speed, and a

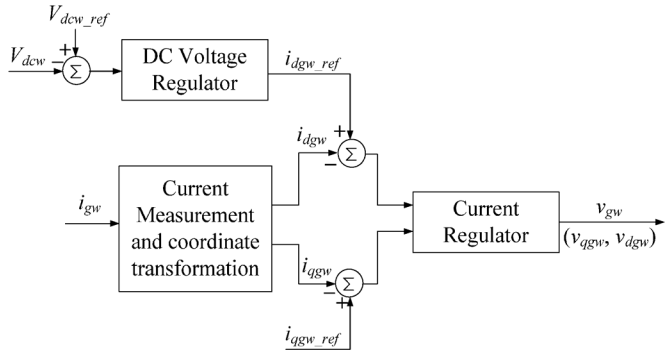

Fig. 2. Control block diagram for the GSC of the studied wind DFIG.

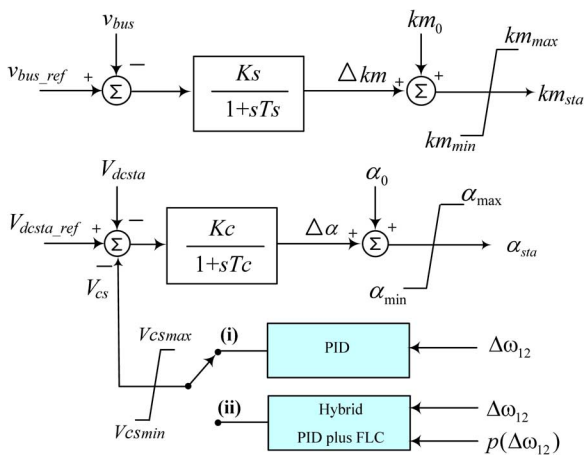

Fig. 3. Control block diagram of the employed STATCOM including the designed PID and hybrid PID plus FLC damping controllers.

noise wind speed [2]. The cut-in, rated, and cut-out wind speeds of the studied VSWT are 4, 14, and 24 m/s, respectively. When $V_W < 14$ m/s, $\beta = 0°$. When $V_W > 14$ m/s, the pitch-angle control system activates to increase β.

The two-inertia reduced-order equivalent mass-spring-damper model of the VSWT coupled to the rotor shaft of the wind DFIG through an equivalent gearbox is used. The per-unit (pu) equations of motion can be referred to [2], [14], and [16].

B. DFIG-Based OWF Model

The stator windings of the studied wind DFIG are directly connected to the low-voltage side of the 0.69/33-kV step-up transformer while the rotor windings of the DFIG are connected to the same 0.69-kV side through a rotor-side converter (RSC), a DC link, a grid-side converter (GSC), and a connection line. For normal operation of a DFIG, the input AC-side voltages of the RSC and the GSC can be effectively controlled to achieve the aims of simultaneous output active-power and reactive-power control [15].

Fig. 2 shows the control block diagram of the RSC, and the operation of the RSC requires i_{qrw} and i_{drw} to follow the varying reference points that are determined by maintaining the output active power and the stator-winding voltage at the setting values, respectively. The required voltage for the RSC (v_{rw}) is derived by controlling the pu q- and d-axis currents of the RSC. The control block diagram of the GSC is shown in Fig. 3. The pu q- and d-axis currents of the GSC, i_{qgw} and i_{dgw}, have to track the reference points that are determined by maintaining the DC link voltage V_{dcw} at the setting value and keeping the output of the GSC at unity power factor, respectively. The required pu voltage of the GSC (v_{gw}) is derived by controlling the per-unit q- and d-axis currents of the GSC [2].

C. STATCOM Model [16]

The pu q- and d-axis output voltages of the proposed STATCOM shown in Fig. 1 can be written by, respectively,

$$v_{qsta} = V_{dcsta} \cdot km_{sta} \cdot \cos(\theta_{bus} + \alpha_{sta}) \quad (5)$$

$$v_{dsta} = V_{dcsta} \cdot km_{sta} \cdot \sin(\theta_{bus} + \alpha_{sta}) \quad (6)$$

where v_{qsta} and v_{dsta} are the pu q- and d-axis voltages at the output terminals of the STATCOM, respectively; km_{sta} and α_{sta} are, respectively, the modulation index and phase angle of the STATCOM; θ_{bus} is the voltage phase angle of the common AC bus, and V_{dcsta} is the pu DC voltage of the DC capacitor C_m. The pu DC voltage-current equation of the DC capacitor C_m can be described by

$$(C_m)p(V_{dcsta}) = \omega_b \left[I_{dcsta} - \left(\frac{V_{dcsta}}{R_m} \right) \right] \quad (7)$$

where p is a differential operator with respect to time t and

$$I_{dcsta} = i_{qsta} \cdot km_{sta} \cdot \cos(\theta_{bus} + \alpha_{sta}) + i_{dsta} \cdot km_{sta} \cdot \sin(\theta_{bus} + \alpha_{sta}) \quad (8)$$

is the pu DC current flowing into the positive terminal of V_{dcsta}, R_m is the pu equivalent resistance considering the equivalent electrical losses of the STATCOM, and i_{qsta} and i_{dsta} are the pu q- and d-axis currents flowing into the terminals of the STATCOM, respectively. The fundamental control block diagram of the employed STATCOM including a PID damping controller is shown in (i) of Fig. 3. The pu DC voltage V_{dcsta} is controlled by α_{sta} while the AC voltage v_{sta} is varied by changing km_{sta}.

D. Three-Machine Nine-Bus System

The well-known three-machine nine-bus power system which is widely used in power system stability studies was shown in Fig. 1. The complete parameters of this system can be referred to [17]. In this paper, each synchronous generator is represented by a two-axis model whose block diagram is shown in Fig. 4. In this model, the transient effects are accounted for while the subtransient effects are neglected. The additional assumptions made in this model are that the transformer-voltage terms in the stator voltage equations are negligible compared to the speed-voltage terms and the rotational speed is approximate to the rated speed of 1.0 pu. The pu differential equations for the i-th synchronous generator are described as follows:

$$\left(\tau'_{qoi}\right) p\left(E'_{di}\right) = -E'_{di} - \left(X_{qi} - X'_{qi}\right) I_{qi} \quad (9)$$

$$\left(\tau'_{doi}\right) p\left(E'_{qi}\right) = -E'_{qi} + E_{FDi} + \left(X_{di} - X'_{di}\right) I_{di} \quad (10)$$

$$(\tau_{ji})p(\omega_i) = T_{mi} - \left[I_{di}E'_{di} + I_{qi}E'_{qi} - \left(L'_{qi} - L'_{di}\right) I_{di} I_{qi}\right] - D_i\omega_i \quad (11)$$

$$p(\delta_i) = \omega_i - 1. \quad (12)$$

Consider the multi-machine system with constant impedance loads shown in Fig. 5 whose network has three generators and three loads. Assume that the three loads are represented by three constant impedances while three generators are represented by

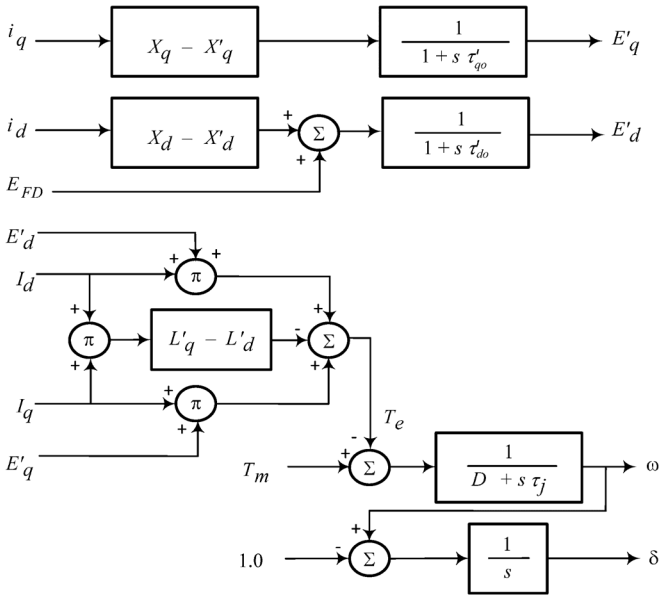

Fig. 4. Block diagram representation of two-axis model for the studied SG.

three active sources. Therefore, all the nodes have zero injection currents except for the generator nodes. This property is used to obtain the network reduction as shown below. With the relation between nodal currents and voltages is

$$\mathbf{I} = \overline{\mathbf{Y}}_{sys}\,\mathbf{V} \tag{13}$$

or

$$\begin{bmatrix} \mathbf{I}_3 \\ \hline \mathbf{0} \end{bmatrix} = \left[\begin{array}{c|c} \mathbf{Y}_{31} & \mathbf{Y}_{32} \\ \hline \mathbf{Y}_{33} & \mathbf{Y}_{34} \end{array}\right] \begin{bmatrix} \mathbf{V}_{31} \\ \mathbf{V}_{32} \end{bmatrix} \tag{14}$$

where $\mathbf{I}_3 = [\overline{I}_{L1}\ \ \overline{I}_{L2}\ \ \overline{I}_{L3}]^T$ is the injected current vector at generator nodes, $\mathbf{V}_{31} = [\overline{V}_1\ \ \overline{V}_2\ \ \overline{V}_3]^T$ is the voltage vector at the generator nodes, $\mathbf{V}_{32} = [\overline{V}_{1'}\ \ \overline{V}_{2'}\ \ \overline{V}_{3'}]^T$ is the voltage vector at the eliminated nodes, and $\mathbf{Y}_{sys}$ is the original system admittance matrix. Expanding the above equations, it yields

$$\mathbf{I}_3 = \mathbf{Y}_{31}\mathbf{V}_{31} + \mathbf{Y}_{32}\mathbf{V}_{32} \text{ and } \mathbf{0} = \mathbf{Y}_{33}\mathbf{V}_{31} + \mathbf{Y}_{34}\mathbf{V}_{32}. \tag{15}$$

From (15), $\mathbf{V}_{32}$ can be eliminated to get

$$\mathbf{I}_3 = \left(\mathbf{Y}_{31} - \mathbf{Y}_{32}\mathbf{Y}_{34}^{-1}\mathbf{Y}_{33}\right)\mathbf{V}_{31} \tag{16}$$

$$\overline{\mathbf{Y}} = \left(\mathbf{Y}_{31} - \mathbf{Y}_{32}\mathbf{Y}_{34}^{-1}\mathbf{Y}_{33}\right) \tag{17}$$

where $\overline{\mathbf{Y}}$ is the desired reduced admittance matrix and it has the dimensions of 3×3. Since each generator is modeled under its own dq-axis reference frame rotating with its rotor, the transformation from each synchronous generator's dq-axis rotor reference frame to the common DQ-axis reference frame is shown in Fig. 6 and can be given as follows:

$$\begin{bmatrix} f_D \\ f_Q \end{bmatrix} = \begin{bmatrix} \sin\delta_i & -\cos\delta_i \\ \cos\delta_i & \sin\delta_i \end{bmatrix} \begin{bmatrix} f_{di} \\ f_{qi} \end{bmatrix} \tag{18}$$

where f can be either a current i or a voltage v while $\delta_{\rm i}$ is the angle between the q-axis of the i-th synchronous generator and the common Q-axis.

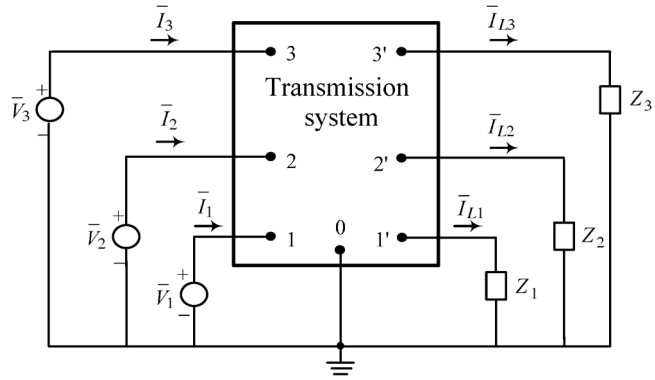

Fig. 5. Multi-machine system with constant impedance loads.

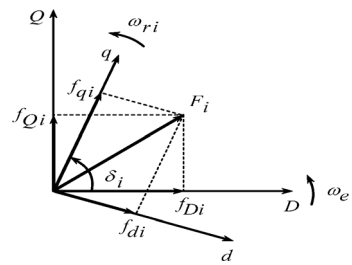

Fig. 6. Transformation from the ith synchronous generator's rotor reference frame to the common DQ reference frame.

III. Design of Damping Controllers for STATCOM

A. Design of a PID Damping Controller

This subsection describes the design procedure and design results of the PID damping controller for the proposed STATCOM to achieve stability improvement of the studied system using a unified approach based on modal control theory. The nonlinear system equations developed in the previous section are linearized around a selected nominal operating point to acquire a set of linearized system equations in matrix form of [16]

$$p\mathbf{X} = \mathbf{A}\mathbf{X} + \mathbf{B}\mathbf{U} + \mathbf{V}\mathbf{W} \tag{19}$$

$$\mathbf{Y} = \mathbf{C}\mathbf{X} + \mathbf{D}\mathbf{U} \tag{20}$$

where $\mathbf{X}$ is the state vector, $\mathbf{Y}$ is the output vector, $\mathbf{U}$ is the external or compensated input vector, $\mathbf{W}$ is the disturbance input vector while $\mathbf{A}$, $\mathbf{B}$, $\mathbf{C}$, and $\mathbf{D}$ are all constant matrices of appropriate dimensions. To design the PID damping controller for the STATCOM, $\mathbf{W}$ in (19) and $\mathbf{U}$ in (20) can be properly ignored by setting $\mathbf{D} = \mathbf{V} = 0$. The state vector $\mathbf{X}$ can be partitioned into three substate vectors as $\mathbf{X} = [\mathbf{X}_{SGs}, \mathbf{X}_{WT-DFIG}, \mathbf{X}_{STATCOM}]^{\rm T}$, where $\mathbf{X}_{SGs}$, $\mathbf{X}_{WT-DFIG}$, and $\mathbf{X}_{STATCOM}$ are referred to the system state vectors of the three SGs, the DFIG-based OWF, and the STATCOM, respectively. Because wind speed V_W seldom reaches the rated wind speed of 14 m/s, V_W of 12 m/s is properly selected as the nominal operating point for designing the PID damping controller. The eigenvalues of the studied three-machine nine-bus system without DFIG-based OWF and with the DFIG-based OWF and the proposed STATCOM are listed in the second and the third columns of Table I, respectively. The eigenvalues $\Lambda_1 - \Lambda_{20}$, $\Lambda_{21} - \Lambda_{33}$, and $\Lambda_{34} - \Lambda_{38}$ listed in Table I relate to the modes of the three-machine nine-bus

system, the DFIG-based OWF system, and the STATCOM, respectively. The following points can be found by examining the system eigenvalues listed in Table I.

1) All modes of the system are almost fixed on the complex plane regardless the addition of the designed PID damping controller for STATCOM.
2) The modes $\Lambda_{1,2}$ and $\Lambda_{3,4}$ relating to the rotor angle deviation between G1 to G2 $(\Delta\delta_{12})$ and the rotor angle deviation between G1 to G3 $(\Delta\delta_{13})$, respectively, are changed and these modes can be improved by damping controllers.

The control block diagram of the STATCOM including the designed PID damping controller was shown in (i) of Fig. 3. The PID damping controller with a first order wash-out term senses the rotor speed deviation of the G1 and G2 $(\Delta\omega_{12})$ to generate a damping signal V_{cs} in order to improve the damping ratios of two modes ($\Lambda_{1,2}$ and $\Lambda_{3,4}$) of studied system listed in Table I. Hence, the output signal in (23) is $\mathbf{Y} = \Delta\omega_{12}$ and $\mathbf{U} = V_{cs}$ is the input vector. The transfer function $H(s)$ of the PID damping controller for the STATCOM in s domain is given by

$$H(s)=\frac{\mathbf{U}(s)}{\mathbf{Y}(s)}=\frac{V_{cs}(s)}{\Delta\omega_{12}(s)}=\frac{sT_W}{1+sT_W}\left(K_P+\frac{K_I}{s}+sK_D\right) \tag{21}$$

where T_W is the time constant of the wash-out term while K_P, K_I, and K_D are the proportional gain, integral gain, and derivative gain of the damping controller, respectively. Taking the Laplace transformation of (19)–(20), the characteristic equation of the closed-loop system containing the PID damping controller can be acquired. The input signal in s domain can be expressed by

$$\mathbf{U}(s) = H(s)\Delta\omega_{12}(s) = H(s)\mathbf{Y}(s) = H(s)\mathbf{C}\mathbf{X}(s). \tag{22}$$

Combining (21)–(22), it yields

$$s\mathbf{X}(s) = \{\mathbf{A} + \mathbf{B}\,[H(s)\mathbf{C}]\}\,\mathbf{X}(s). \tag{23}$$

The characteristic equation of the closed-loop system including the PID damping controller is given by

$$\det\{s\mathbf{I} - [\mathbf{A} + \mathbf{B}H(s)\mathbf{C}]\} = 0. \tag{24}$$

When two pairs of the specified mechanical modes ($\Lambda_{1,2}$ and $\Lambda_{3,4}$) are substituted into (24), the four parameters of the PID controller can be obtained. The design results of the PID damping controller for the STATCOM are given as below.

Prespecified Eigenvalues

$$\Lambda_{1,2} = -0.85 \pm j14 \text{ and } \Lambda_{3,4} = -0.90 \pm j8.0.$$

Parameters of the Designed PID Damping Controller

$$K_P = -47.21, K_I == -183.23,\ K_D = -33.36,\ \text{and } T_W = 0.42 \text{ s}.$$

The eigenvalues of the studied three-machine nine-bus system containing the DFIG-based OWF and the proposed STATCOM joined with the designed PID damping controller are listed in the fourth column of Table I. It can be clearly observed that both $\Lambda_{1,2}$ and $\Lambda_{3,4}$ have been exactly positioned on the desired locations on the complex plane. Moreover, the damping ratios of $\Lambda_{1,2}$ and $\Lambda_{3,4}$ increase from 0.03842 to 0.06060 and from 0.06824 to 0.11179, respectively. Some major constraints for selecting the assigned eigenvalues can be referred to [16] and [18]. According to the eigenvalue results listed in the fourth column of Table I and the four parameters of the designed PID damping controller of the STATCOM shown above, it can be concluded that the design results are appropriate to the studied system.

TABLE I
EIGENVALUES (rad/s) [DAMPING RATIOS] OF THE STUDIED SYSTEM UNDER WIND SPEED OF 12 m/s

Eigenvalue No.	System without OWF and STATCOM	System with OWF and STATCOM	System with OWF, STATCOM and PID controller
$\Lambda_{1,2}$	-0.64457 ± *j*12.643 [0.050916]	-0.5483 ± *j*14.142 [0.03842]	**-0.85 ± *j*14.0*** [0.06060]
$\Lambda_{3,4}$	-0.62939 ± *j*8.8714 [0.07076]	-0.5533 ± *j* 8.089 [0.06824]	**-0.90 ± *j*8.0*** [0.11179]
$\Lambda_{5,6}$	-5.2056 ± *j*7.8469	-5.2686 ± *j*7.8815	-5.2676 ± *j*7.8901
$\Lambda_{7,8}$	-5.2419 ± *j*7.9464	-5.2483 ± *j*7.943	-5.2745 ± *j*7.9325
$\Lambda_{9,10}$	-5.2479 ± *j*7.9823	-5.3696 ± *j*7.9535	-5.3844 ± *j*7.9657
$\Lambda_{11,12}$	-6.4894, -3.9926	-7.0012, -3.646	-7.4325 ± *j*0.7794
$\Lambda_{13,14}$	-0.44061 ± *j*0.9991	-0.4939 ± *j*0.8039	-0.3258 ± *j*0.8786
$\Lambda_{15,16}$	-0.38165 ± *j*0.5615	-0.3706 ± *j*0.5521	-0.3658 ± *j*0.6498
$\Lambda_{17,18}$	-0.34982 ± *j*0.3445	-0.2404 ± *j*0.1145	-0.1812 ± *j*0.1461
$\Lambda_{19,20}$	-3.2258, -0.3732	-0.2388, -3.2258	-0.2388, -3.2258
$\Lambda_{21,22}$	-	-87.568 ± *j*179.18	-87.505 ± *j*179.07
$\Lambda_{23,24}$	-	-56.093 ± *j*141.12	-56.067 ± *j*141.13
$\Lambda_{25,26}$	-	-116.42 ± *j*91.274	-116.45 ± *j*91.251
$\Lambda_{27,28}$	-	-64.781, -41.788	-64.765, -35.564
$\Lambda_{29,30}$	-	-5.7815 ± *j*15.451	-5.7816 ± *j*15.451
$\Lambda_{31,32}$	-	-28.55, -12.845	-28.555, -12.815
Λ_{33}	-	-1.9628	-1.6891
$\Lambda_{34,35}$	-	-99.742, -100.12	-100.02, -99.403
$\Lambda_{36,37}$	-	-0.131 ± *j*0.5424	-0.331 ± *j*0.1837
Λ_{38}	-	-0.25609	-0.23011
Λ_{39}	-	-	-3.7109

* denotes exactly assigned eigenvalues

B. Design of an FLC Plus to the Designed PID

This section employs the technique of FLC theorem to design the hybrid PID plus FLC damping controller shown in (ii) of Fig. 3. To design the FLC controller, the following fundamental design steps for a FLC are employed and referred to [19] including: 1) fuzzification (FI), 2) decision-making logic (DML), 3) defuzzification (DFI), and 4) knowledge base (KB). Fig. 7 plots the block diagram of this hybrid control system, where the rotor-speed deviation between G1 and G2, $\Delta\omega_{12}$, and its derivative, $p(\Delta\omega_{12})$, are fed to the FLC to generate three auxiliary gains (K'_P, K'_I, and K'_D) for adding to the three gains of the designed PID controller (K_P, K_I, and K_D) in the previous subsection to control the phase angle (α_{sta}) of the STATCOM. These incremental gains from the FLC are updated to the gains of the PID controller using the following rules [12]:

$$K_{Ph} = K_P + K'_P \tag{25}$$

$$K_{Ih} = K_I + K'_I \tag{26}$$

$$K_{Dh} = K_D + K'_D. \tag{27}$$

This paper utilizes the Sugeno-type fuzzy inference system since it works well with linear, optimization, and adaptive techniques [10], [11]. Seven linguistic variables for each input variable are used. These are NB (Negative Big), NM (Negative Medium), NS (Negative Small), ZR (Zero), PS (Positive Small), PM (Positive Medium), and PB (Positive Big). There are also seven linguistic variables for output variable, namely, IB (Increase Big), IM (Increase Medium), IS (Increase Small), KV (Keep Value), DS (Decrease Small), DM (Decrease Medium),

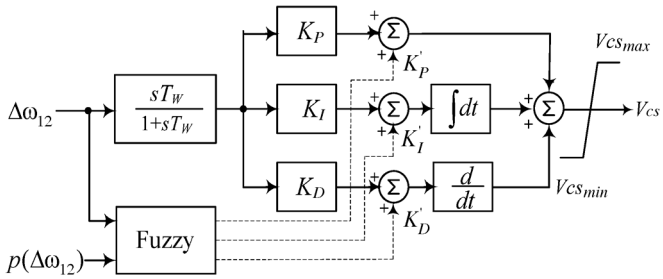

Fig. 7. Block diagram of the proposed hybrid PID plus FLC.

TABLE II
CONTROL RULES OF THE STUDIED FLC

Δω12 / p(Δω12)	NB	NM	NS	ZR	PS	PM	PB
PB	KV	IS	IM	IB	IB	IB	IB
PM	DS	KV	IS	IM	IB	IB	IB
PS	DM	DS	KV	IS	IM	IB	IB
ZR	DB	DM	DS	KV	IS	IM	IB
NS	DB	DB	DM	DS	KV	IS	IM
NM	DB	DB	DB	DM	DS	KV	IS
NB	DB	DB	DB	DB	DM	DS	KV

and DB (Decrease Big). The control rules subject to the two input signals and the output signal are listed in Table II.

IV. Root-Loci Analysis Under Various Operating Conditions

This section presents the comparative root-loci analyzed results of the system dominant modes when the proposed STATCOM is with and without the designed PID damping controller under widely changed wind speeds. The simulated wind speed V_W of the DFIG-based OWF is increased from 4 m/s (cut-in wind speed of VSWT) to 24 m/s (cut-out wind speed of VSWT). Fig. 8(a) and (b) shows the corresponding root-loci plots for the eigenvalues of the rotor angle between G1 to G2 (δ_{12}) and the rotor angle between G1 to G3 (δ_{13}) under the selected wind speeds, respectively. It is found that these dominant modes can maintain stable operation and move to leftward of the imaginary axis when the designed PID controller is in service. It means that the system is more stable when the proposed STATCOM is with the designed PID controller.

V. Nonlinear Model Simulations

This section uses the nonlinear system model developed in Section II to compare the damping characteristics contributed by the proposed STATCOM joined with the designed PID damping controller and the hybrid PID plus FLC damping controller on stability improvement of the studied system under a three-phase short-circuit fault at bus 9 of Fig. 1. The three-phase short-circuit fault is suddenly applied to bus 9 at $t = 1$ s and is cleared at $t = 1.1$ s. Although this type of fault seldom occurs in practical power systems, it is the most critical and the most severe fault to check whether the studied systems can withstand such severe system impacts. If the studied systems are stable when this severe fault is suddenly applied and is cleared by some protective relays, it means that the studied systems have ability to remain stable operation when the systems are subject to other faults such as single line-to-ground fault, line-to-line fault, etc. It is assumed that the DFIG-based OWF operates

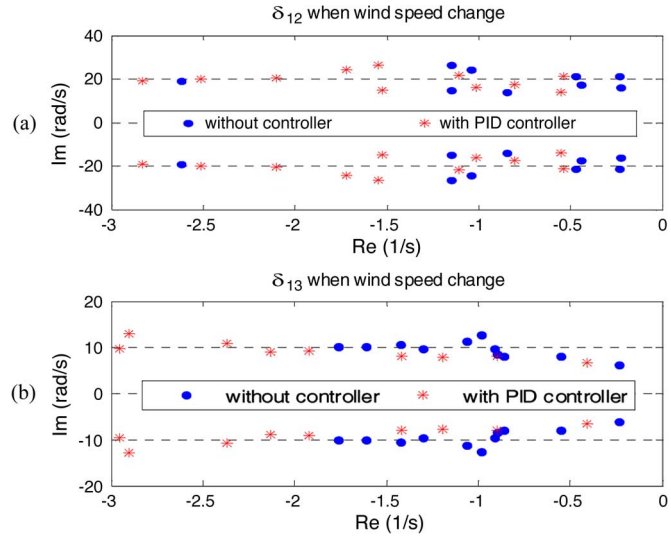

Fig. 8. Root-loci results of the studied system versus various values of wind speed condition.

under a base wind speed of 12 m/s while the three-machine system operates under a stable condition as referred to [17] and [20]. The simulation results of the proposed system using MATLAB/SIMULINK toolbox are presented in Fig. 9. This figure plots the comparative transient responses of the studied system with the proposed STATCOM without controller (blue lines), with the designed PID damping controller (red lines) and with the hybrid PID plus FLC damping controller (black lines). It is clearly observed from the comparative transient simulation results shown in Fig. 9 that the proposed STATCOM with the designed hybrid PID plus FLC damping controller can offer better damping characteristics than the designed PID damping controller.

The rotor speeds and the rotor angle derivations of the three SGs are shown in Fig. 9(a)–(e), respectively. While terminal voltages of each SG are plotted, respectively, in Fig. 9(g)–(i). For the responses of the DFIG-based OWF, the rotor speed and terminal voltage of the DFIG are plotted in Fig. 9(f) and (j), respectively. Fig. 9(k) presents the reactive power of the STATCOM. It is obviously seen that the damping of the studied system is still very poor with the stable time of about 6 s when the STATCOM is connected to the connected bus (bus 9). By coordinating with the designed PID damping controller with the STATCOM, the studied system has better damping and it is stable at around $t = 4$ s.

For more clearly, the percentage of improvement index (μ) is used. The transient responses shown in Fig. 9 are assumed to be similar to the transient responses of a typical second-order system as shown in Fig. 10. The overshoot refers to an output exceeding its steady-state value and percent of overshoot (POT) is an index to qualify the overshoot of a system, POT is calculated as follows:

$$\text{POT} = \frac{y_{max} - y_{ss}}{y_{ss}} \times 100\% \tag{28}$$

where y_{max} and y_{ss} are the maximum and steady-state values of y, respectively. Applying (28), the percentage of improvement (μ) of each figure is calculated and the result is also shown in Fig. 9 when the studied system is without controller and with the designed PID+FLC controller. It can be observed that only

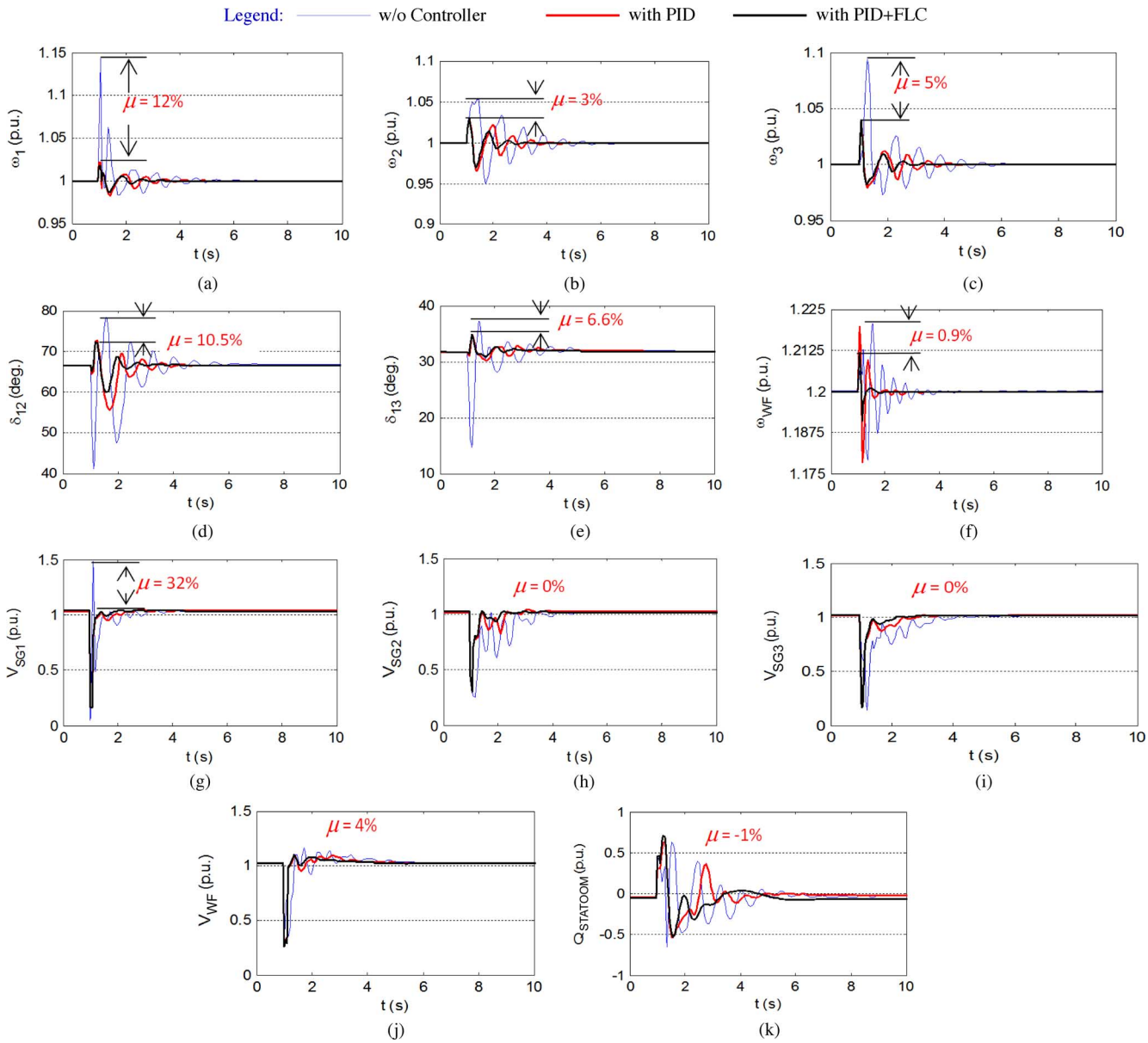

Fig. 9. Transient responses of the studied system under a three-phase short-circuit fault happened at bus 9. (a) Rotor speed of G1; (b) rotor speed of G2; (c) rotor speed of G3; (d) rotor angle deviation between G1 to G2; (e) rotor angle deviation between G1 to G3; (f) rotor speed of equivalent DFIG-based OWF; (g) terminal voltage of G1; (h) terminal voltage of G2; (i) terminal voltage of G3; (j) voltage of OWF; (k) reactive power supplied by STATCOM.

Fig. 9(k) (reactive power supplied by STATCOM) has a very small negative value for μ of -1%. However, most responses shown in Fig. 9 demonstrate better damping and stable time when the studied system is with the designed PID+FLC controller.

It shows that the proposed STATCOM with the designed PID and hybrid PID plus FLC damping controllers can supply proper reactive power to the studied system and offer better damping characteristics to quickly damp out the inherent oscillations of the studied system than the studied system without controller.

VI. Conclusion

This paper has presented the stability improvement of a DFIG-based OWF fed to a multi-machine system using a STATCOM. The STATCOM is proposed and is connected to the connected bus of the OWF to the multi-machine system. To supply the adequate reactive power to the system, a PID damping controller for the STATCOM has been designed by using a modal control theory to assign two dominant modes of the studied system to the desired locations on the complex

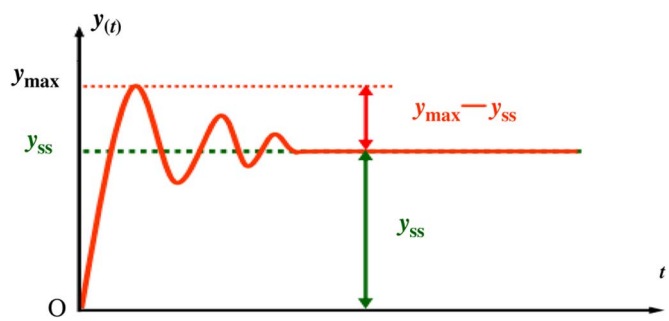

Fig. 10. Transient response of a typical second-order system.

plane. Root-loci plots under various wind speed operating conditions have been carried to show the effectiveness of the designed PID damping controller. Moreover, for improving the performance of the studied system with the designed PID, a hybrid PID plus FLC damping controller is also designed. Comparative time-domain simulations of the studied system subject to a three-phase short-circuit fault at the connected bus have been systematically performed to demonstrate the effectiveness of the proposed STATCOM joined with the two designed damping controllers on suppressing inherent oscillations of the studied system. It can be concluded from the simulation results that the proposed STATCOM joined with the designed hybrid PID plus FLC damping controller has the best damping characteristics to improve the performance of the DFIG-based OWF fed to the studied multi-machine system under different operating conditions.

REFERENCES

[1] R. Pena, J. C. Clare, and G. M. Asher, "Doubly fed induction generator using back-to-back PWM converters and its application to variable speed wind-energy generation," *Proc. Inst. Elect. Eng., Elect. Power Appl.*, vol. 143, no. 3, pp. 231–241, May 1996.

[2] L. Wang and K.-H. Wang, "Dynamic stability analysis of a DFIG-based offshore wind farm connected to a power grid through an HVDC link," *IEEE Trans. Power Syst.*, vol. 26, no. 3, pp. 1501–1510, Aug. 2010.

[3] L. Wang and L.-Y. Chen, "Reduction of power fluctuations of a large-scale grid-connected offshore wind farm using a variable frequency transformer," *IEEE Trans. Sustain. Energy*, vol. 2, no. 3, pp. 226–234, Apr. 2011.

[4] E. Muljadi, T. B. Nguyen, and M. A. Pai, "Impact of wind power plants on voltage and transient stability of power systems," in *Proc. IEEE Energy 2030 Conf.*, Nov. 2008, pp. 1–7.

[5] O. Anaya-Lara, A. Arulampalam, G. Bathurst, F. M. Hughes, and N. Jenkins, "Transient analysis of DFIG wind turbines in multi-machine networks," in *Proc. 18th Int. Conf. Exhib. Electricity Distribution CIRED*, Jun. 2005, pp. 1–5.

[6] K. E. Okedu, S. M. Muyeen, R. Takahashi, and J. Tamura, "Improvement of fault ride through capability of wind farms using DFIG considering SDBR," in *Proc. 14th Eur. Conf. Power Electronics and Applications*, Sep. 2011, pp. 1–10.

[7] N. G. Hingorani and L. Gyugyi, *Understanding FACTS; Concepts and Technology of Flexible AC Transmission Systems*. New York, NY, USA: IEEE Press, 2000.

[8] B. Pokharel and W. Gao, "Mitigation of disturbances in DFIG-based wind farm connected to weak distribution system using STATCOM," in *Proc. North American Power Symp. (NAPS)*, Sep. 26–28, 2010, pp. 1–7.

[9] G. Cai, C. Liu, Q. Sun, D. Yang, and P. Li, "A new control strategy to improve voltage stability of the power system containing large-scale wind power plants," in *Proc. 4th Int. Conf. Electric Utility Deregulation and Restructuring and Power Technologies (DRPT)*, Jul. 2011, pp. 1276–1281.

[10] M. N. Eskander and S. I. Amer, "Mitigation of voltage dips and swells in grid-connected wind energy conversion systems," in *Proc. ICCAS-SICE*, Aug. 2009, pp. 885–890.

[11] L. O. Mak, Y. X. Ni, and C. M. Shen, "STATCOM with fuzzy controllers for interconnected power systems," *Elect. Power Syst. Res.*, vol. 55, no. 2, pp. 87–95, Aug. 2000.

[12] M. N. Uddin and R. S. Rebeiro, "Improved dynamic and steady state performance of a hybrid speed controller based IPMSM drive," in *Proc. IEEE Industry Applications Society Annual Meeting (IAS)*, Oct. 9–13, 2011, pp. 1–8.

[13] L. Reznik, O. Ghanayem, and A. Bourmistrov, "PID plus fuzzy controller structures as a design base for industrial applications," *Eng. Appl. Artif. Intell.*, vol. 13, no. 4, pp. 419–430, Aug. 2000.

[14] S. M. Muyeen, M. H. Ali, R. Takahashi, T. Murata, J. Tamura, Y. Tomaki, A. Sakahara, and E. Sasano, "Transient stability analysis of wind generator system with the consideration of multi-mass shaft model," in *Proc. Int. Conf. Power Electronics and Drives Systems*, Jan. 16–18, 2006, vol. 1, pp. 511–516.

[15] P. Cartwright, L. Holdsworth, J. B. Ekanayake, and N. Jenkins, "Co-ordinated voltage control strategy for a doubly-fed induction generator (DFIG)-Based wind farm," *Proc. Inst. Elect. Eng., Gener., Transm., Distrib.*, vol. 151, no. 4, pp. 495–502, Aug. 2004.

[16] L. Wang and C.-T. Hsiung, "Dynamic stability improvement of an integrated grid-connected offshore wind farm and marine-current farm using a STATCOM," *IEEE Trans. Power Syst.*, vol. 26, no. 2, pp. 690–698, May 2011.

[17] P. M. Anderson and A. A. Fouad, *Power System Control and Stability*. Ames, IA, USA: Iowa State Univ. Press, 1977.

[18] J. Ma, Z. Y. Dong, and P. Zhang, "Eigenvalue sensitivity analysis for dynamic power system," in *Proc. Int. Conf. Power System Technology*, Oct. 22–26, 2006, pp. 1–7.

[19] C. C. Lee, "Fuzzy logic in control system: Fuzzy logic controller, Part I and II," *IEEE Trans. System, Man, Cybern.*, vol. 20, pp. 404–435, Mar./Apr. 1990.

[20] P. W. Sauer and M. A. Pai, *Power System Dynamics and Stability*. Englewood Cliffs, NJ, USA: Prentice Hall, 1998.

Li Wang (S'87–M'88–SM'05) received the Ph.D. degree from the Department of Electrical Engineering, National Taiwan University, Taipei City, Taiwan, in June 1988.

He has been an associated professor and a professor at the Department of Electrical Engineering, National Cheng Kung University, Tainan City, Taiwan, in 1988 and 1995, respectively. He was a visiting scholar of the School of Electrical Engineering and Computer Science, Purdue University, West Lafayette, IN, USA, from February 2000 to July 2000, and the School of Electrical Engineering and Computer Science, Washington State University, Pullman, WA, USA, from August 2003 to January 2004. He was a research scholar of the Energy Systems Research Center (ESRC), the University of Texas at Arlington (UTA), Arlington, TX, USA, from July 2008 to January 2009. At present, his research interests include power systems dynamics, power system stability, AC machine analyses, and renewable energy.

Dinh-Nhon Truong was born in Quang nam Province, Vietnam, on December 3, 1979. He received the B.S. and M.S. degrees from the Department of Electrical and Electronics Engineering, University of Technical Education, Ho Chi Minh City, Vietnam, in April 2003 and May 2005, respectively. He is currently pursuing the Ph.D. degree at the Department of Electrical Engineering, National Cheng Kung University, Tainan, Taiwan.

His research interests are grid-connected wind power systems and marine-current energy conversion systems.